第 51 卷 第 2 期/2024 年 1 月/中国激光 研究论文

中国激光

基于小孔径光阑整形的低损耗飞秒光纤光栅制备

张鹏浩[1]，武洪波[1]，陈爽[1]，江文松[2*]，张力[1]

[1]中国航空工业集团有限公司北京长城计量测试技术研究所，北京 100095；

[2]中国计量大学计量测试工程学院，浙江 杭州 310018

摘要 针对飞秒激光逐点法制备的光纤布拉格光栅(FBG)损耗较大的问题，提出了一种基于小孔径光阑整形的低损耗飞秒光纤光栅制备方法。首先分析了孔径光阑限制下聚焦高斯光束焦场的能量分布，利用小孔径光阑整形获得了丝状焦场的孔径条件。利用小孔径光阑整形的飞秒激光刻写装置制备FBG，在光阑孔径由10 mm逐步降低至1 mm的过程中，光栅条纹形态由圆形过渡到丝状，丝状光栅条纹对入射光的散射更弱、耦合效率更高，使插入损耗由0.90 dB降低至0.11 dB，短波损耗由4.01 dB降低至0.35 dB。受包层模与纤芯模耦合的影响，短波损耗以振荡形式存在，实验验证了涂覆层和低反射率对振荡的抑制作用。

关键词 光栅；光纤布拉格光栅；飞秒激光；小孔径光阑；插入损耗；短波损耗

中图分类号 O436 **文献标志码** A **DOI**：10.3788/CJL230747

1 引 言

光纤布拉格光栅(FBG)具有体积小、质量轻、灵敏度高、抗电磁干扰和复用能力强等优点，作为传感器的关键敏感元件，在航空航天、核电冶金以及桥梁隧道等诸多领域中具有广泛的应用[1-3]。飞秒激光借助极高的峰值功率和极短的脉冲时间，可直接在光纤纤芯诱导产生Type II型的折射率调制，制备的FBG具有很高的机械强度和热稳定性[4-5]。飞秒激光结合相位掩模板法[6]或逐点法是两种常见的FBG制备方法，其中逐点法以其高灵活性的优势，被广泛应用于切趾[7-8]、啁啾[9]甚至更复杂光谱形态FBG的制备[9-12]。

利用飞秒激光逐点法制备的FBG通常有较大的损耗，表现为插入损耗和短波损耗等多种形式，严重影响光栅性能。Åslund等[13]研究了损耗的形成机理，实验结果表明，损耗主要来源于光栅条纹表面对入射光的米氏散射，通过改变光栅尺寸和形态，可改变光栅与入射模式之间的重叠积分，进而损耗得到抑制。为了降低逐点法制备FBG的损耗，研究人员从刻写路径、飞秒激光光斑整形和特种光纤等多个方面进行了改进。在刻写路径方面，将逐点法改进为逐线法，即先沿光纤径向逐点扫描成线，再沿光纤轴向用线阵列构成光栅，获得高反射率和低插入损耗的FBG，不过由点成线的过程显著增加了制备时长[14]。逐面法是在逐点法光路中加入狭缝，以损失部分激光能量为代价，将光纤横截面内焦点附近的光斑展宽为平面以刻写FBG[15-16]，将插入损耗降低至0.3 dB[17]。Williams等[18]提出了一种基于压电振动台的连续扫描法，在垂直于飞秒激光入射方向和光纤移动方向上，一维压电振动台承载着光纤按照设定频率振动，制备出具有极低插入损耗(约0.1 dB)的高反射率FBG。这种连续扫描技术可实现大范围的材料改性，有利于制备大模场光纤光栅，不过二维移动提高了装置复杂程度。Wang等[19]选用细芯单模光纤，利用飞秒激光逐点法在其纤芯处制备了准分布式FBG，结果表明，细芯FBG的插入损耗约为0.25 dB，短波损耗小于具有相同反射率的标准芯径FBG，但细芯光纤与常用的标准石英单模光纤的熔接耦合容易损失光能量，较细的纤芯也提高了飞秒激光聚焦和光纤对准的难度。

本文提出了一种基于小孔径光阑整形的低损耗飞秒光纤光栅制备方法。首先分析了孔径光阑限制下高斯光束焦场的能量分布，通过小孔径光阑整形获得了丝状焦场。在逐点法的基础上，搭建了小孔径光阑整形的飞秒激光刻写装置。利用10.0～0.5 mm不同孔径的光阑制备了反射率为90%左右、中心波长在1550 nm附近的FBG，通过对比FBG条纹形态以及透射光谱中的损耗特性，验证了小孔径光阑法的丝状整形效果以及对插入损耗和短波损耗的抑制作用。通过分析包层模激发原理，阐明了短波损耗以振荡形式存在的原因，实验验证了涂覆层和低反射率的FBG对振荡的抑制效果。

收稿日期：2023-04-19；**修回日期**：2023-05-17；**录用日期**：2023-05-24；**网络首发日期**：2023-07-04

基金项目：国家自然科学基金(52005471)、国家重点研发计划(2022YFF0705704)

通信作者：*jwensong@cjlu.edu.cn

2 基本原理

基于小孔径光阑整形的逐点法制备FBG的原理如图1所示。飞秒激光沿z方向入射，由于飞秒激光器直接输出的激光光斑能量密度低，需要对光束进行聚焦以达到刻写FBG所需的能量密度。为了消除光纤圆柱形的表面对入射激光的散焦效应，将光纤置于匹配液中，并在表面覆盖盖玻片。光纤在高精密位移台的带动下沿光纤轴向(x方向)匀速运动，飞秒激光脉冲逐点调制纤芯的折射率，形成周期性的条纹阵列，构成FBG。本方法在光束聚焦前插入小孔径光阑，减小入射光束进入聚焦物镜的光斑直径(ω)，同时不会改变聚焦物镜的焦距(f)，从而聚焦物镜的数值孔径(NA)减小为

$$NA = n \cdot \frac{1}{\sqrt{1+\left(\frac{f}{\omega}\right)^2}}, \tag{1}$$

式中：n为聚焦介质的折射率。

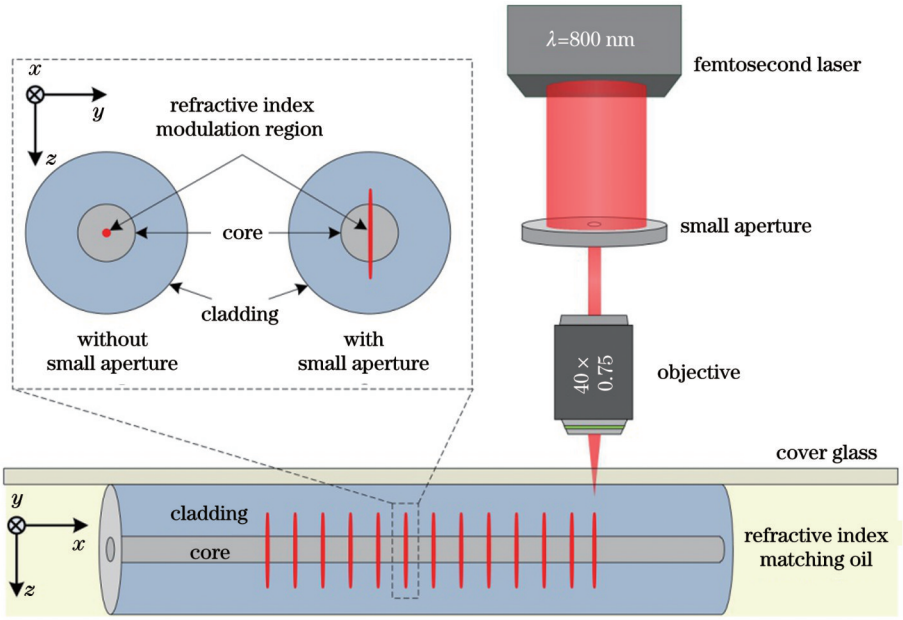

图1 基于小孔径光阑整形逐点制备光纤布拉格光栅的原理图

Fig. 1 Schematic of point-by-point fabrication of FBG based on beam shaping by small aperture

为了研究数值孔径对高斯光束聚焦焦场能量分布的影响，飞秒激光的聚焦过程可简化为一束平行高斯光束经过聚焦物镜进行聚焦，将高斯光束的椭圆形光斑近似为圆形光斑，焦点处的束腰半径为

$$\omega_0 = \frac{\lambda}{\pi \cdot NA}, \tag{2}$$

式中：λ为高斯光束在介质中的波长。焦点处的瑞利长度为

$$Z_0 = \frac{\pi\omega_0^2}{\lambda}。 \tag{3}$$

焦点处能量分布[20]为

$$I(x,y,z) = I_0\left[\frac{\omega_0}{\omega(z)}\right]\exp\left[-\frac{2(x^2+y^2)}{\omega^2(z)}\right], \tag{4}$$

式中：(x,y,z)为坐标；I_0为归一化光强度；$\omega(z)$为距离焦点z处的光斑直径，$\omega(z)=\omega_0\sqrt{1+(z/Z_0)^2}$。

根据式(2)、(3)计算10.0～0.5 mm孔径光阑焦点处的束腰半径和瑞利长度(以光强降低至$1/e^2$作为截止条件)，结果如图2所示，随着光阑孔径的减小，束腰半径和瑞利长度逐步增大。根据式(4)分别计算光

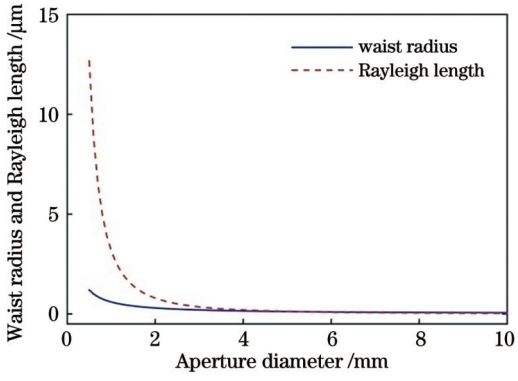

图2 束腰半径和瑞利长度随光阑孔径的变化

Fig. 2 Waist radius and Rayleigh length versus aperture of diaphragm

阑孔径为10.0 mm和1.0 mm时光纤横截面(y-z平面)内的焦场能量分布，结果如图3所示，其在整体上是以焦点为中心的高斯分布。当光阑孔径较大时，数值孔径较大，焦场瑞利长度较短，形态接近圆形；当光阑孔径较小时，数值孔径较小，由于瑞利长度的增长幅度快于束腰半径，焦场的形态更加狭长，更接近丝状。

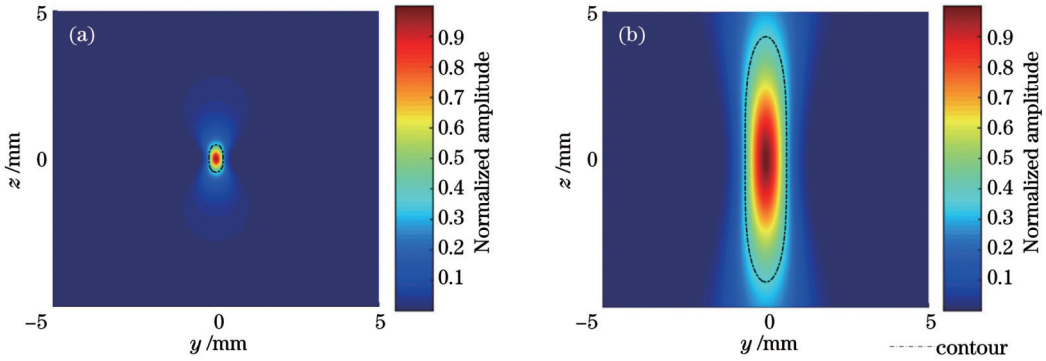

图 3　焦场能量分布。(a)光阑孔径为 10.0 mm;(b)光阑孔径为 1.0 mm

Fig. 3　Focal field energy distributions. (a) Aperture of 10.0 mm; (b) aperture of 1.0 mm

3　实验结果与讨论

采用掺钛蓝宝石飞秒激光器作为光源,飞秒激光的中心波长为 800 nm,脉冲宽度为 120 fs,重复频率为 1 kHz,最大单脉冲能量约为 1 mJ,光斑直径约为 10 mm。物镜的放大倍数为 40 倍,数值孔径 *NA* 为 0.75。光纤为标准石英单模光纤,纤芯直径为 8.2 μm,包层直径为 125 μm,涂覆层为丙烯酸酯,厚度约为 62 μm。刻制长度为 3 mm 的 2 阶 FBG,刻制前剥除光纤涂覆层。

利用光纤光栅解调仪监测 FBG 的透射光谱,波长范围为 1510～1590 nm,波长分辨力为 1 pm。采用图 4 所示方法的测试 FBG 透射光谱。首先测试光纤光栅解调仪光源的透射光谱,光源发出的激光经环形器、光纤适配器、单模光纤等进入接收端,记为光源透射光谱。然后将跳线从中间剪断,将 FBG 熔接进跳线中,记录为预测试 FBG 透射光谱。将预测试 FBG 透射光谱减去光源透射光谱,获得最终的 FBG 透射光谱。测试过程中需要保证全链路的插接状态稳定。该测试方法能够有效避免光源光谱不平坦和链路插接损耗等对测试结果的影响。

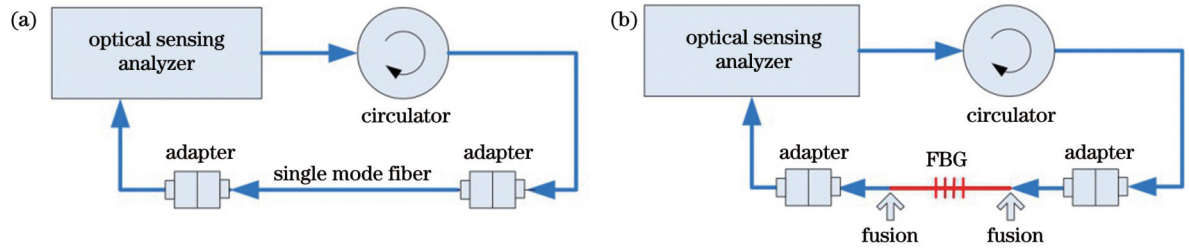

图 4　FBG 透射光谱测试方法。(a)测试光源透射光谱;(b)预测试 FBG 透射光谱

Fig. 4　Test method for FBG transmission spectrum. (a) Test of light source transmission spectrum; (b) pretest of FBG transmission spectrum

采用 10.0、5.0、2.5、1.0、0.5 mm 不同孔径的光阑制备 FBG。为了对比不同孔径下 FBG 的损耗,调节刻制每支 FBG 使用的单脉冲能量,使 FBG 的反射率均在 90% 左右,中心波长在 1550 nm 附近。在电荷耦合器件(CCD)相机下观察到的 FBG 显微图像以及对应的透射光谱如图 5 所示。随着光阑孔径的减小,在飞秒激光入射方向上[图 5(a)～(e)]和垂直于飞秒激光入射方向上[图 5(f)～(j)],观察到的光栅条纹长度都呈逐步增大的趋势,垂直入射方向的增大速度显著快于入射方向。当光阑孔径为 10.0 mm 时,高数值孔径使飞秒激光的焦场能量分布接近圆形,诱导形成了高度局域化的折射率调制区域,具体表现为两个方向上观察到的光栅条纹长度基本相同,分别为 1.37 μm 和 1.74 μm[图 5(a)、(f)],光栅条纹形态也接近圆形。光阑孔径为 5.0 mm 时的状态与 10.0 mm 时基本一致。当光阑孔径降低至 2.5 mm 时,在垂直于飞秒激光入射方向上观察到的光栅条纹被拉长到 4.93 μm[图 5(h)]。当光阑孔径进一步降低至 1.0 mm 和 0.5 mm 时,小孔径光阑将焦场能量分布整形为丝状,受此影响,光栅条纹被进一步拉长,达到 15.23 μm 和 21.34 μm[图 5(i)、(j)],此时的光栅条纹形态已呈丝状。另外,光栅条纹的颜色中间深、两端浅,这是由于焦场能量呈高斯分布,诱导产生的折射率调制区域同样为高斯型,在焦点正中折射率调制幅度最大,对应的颜色也最深[21]。

由图 5(k)～(o)所示的透射光谱可以看出,当光阑孔径大于等于 1.0 mm 时,随着光阑孔径的减小,FBG 的插入损耗和短波损耗整体上呈逐渐减小的趋势。例如,当光阑孔径为 10.0 mm 时,插入损耗和 1510 nm 处的短波损耗分别为 0.90 dB 和 4.01 dB;当光阑孔径减小至 1.0 mm 时,两种损耗分别降低至 0.11 dB 和 0.35 dB。实验结果表明,小孔径光阑对损耗产生了显著的抑制效果。这主要得益于圆形光栅条纹被整形为

丝状：一方面丝状光栅条纹降低了原圆形表面曲率，减少了对入射光的米氏散射；另一方面根据耦合模理论[22-23]，相比圆形光栅条纹，丝状光栅条纹与基模电场耦合的面积更大，产生相同交流耦合强度所需的折射率调制量更小，米氏散射也更弱。通过对比光栅条纹的明暗程度来观察折射率调制量的变化。相比孔径为1.0 mm的光阑[图5(d)、(i)]，当光阑孔径为10.0 mm时[图5(a)、(f)]，光栅条纹轮廓更清晰、明锐。但是当进一步减小光阑孔径至0.5 mm时，插入损耗和在1510 nm处的短波损耗出现增大的反常现象[图5(o)]。这主要是焦点处的束腰半径增大，相邻光栅条纹出现了部分重叠[图5(e)]。为了制备反射率高达90%的FBG，需要提高单脉冲激光能量以产生更高幅度的折射率调制，调制与未调制区域之间更高的折射率差增

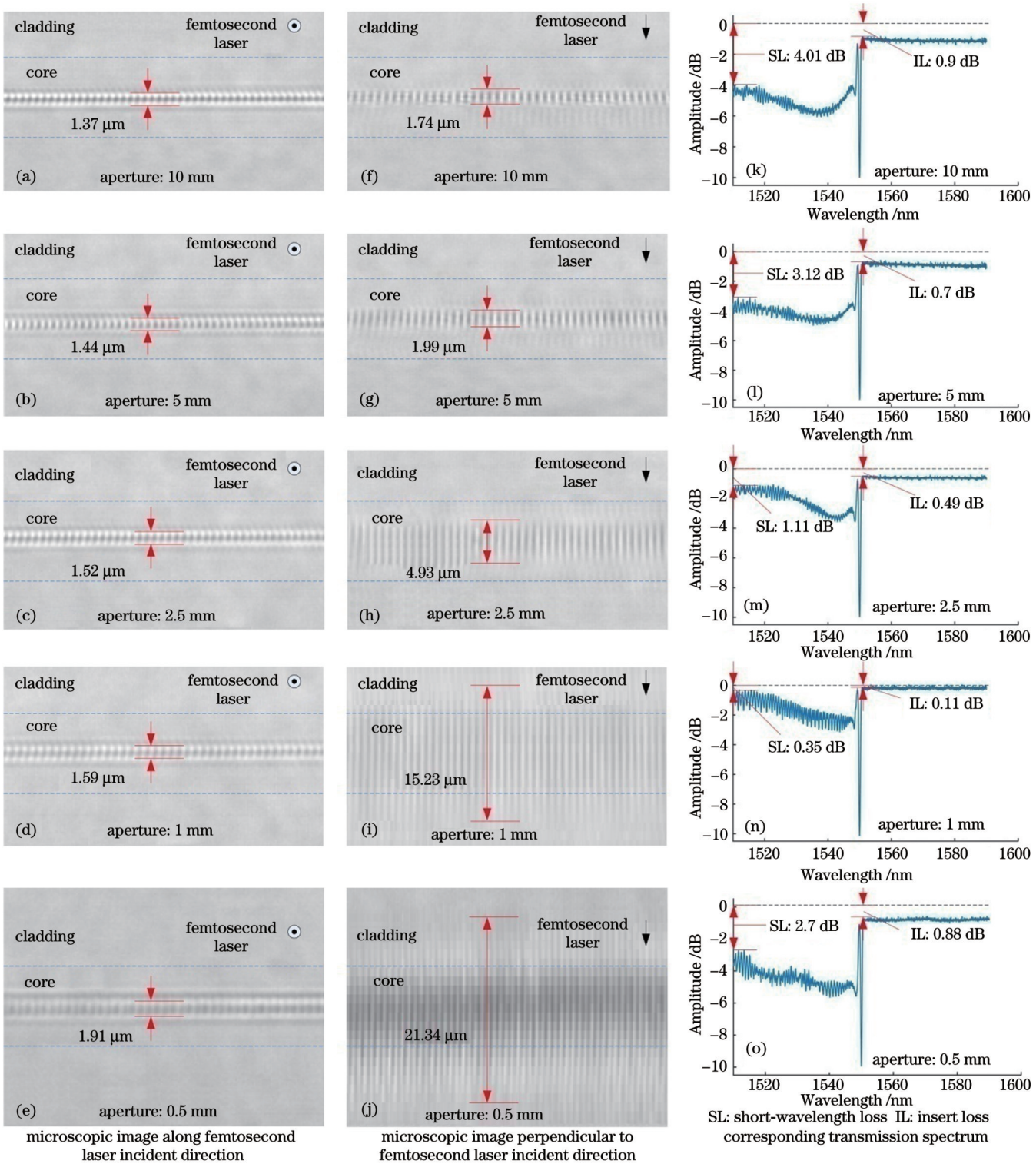

图5 不同孔径光阑制备的FBG的显微图像及对应的透射光谱

Fig. 5 Microscopic images of FBG fabricated with different apertures and corresponding transmission spectra

强了光栅条纹对入射光的米氏散射，从而引起了更大的损耗。通过提高FBG的阶数，增大条纹间隔，可以避免相邻条纹重叠，但是条纹数量将减少，光谱带宽将展宽[23]，这不利于FBG的实际应用。

为了详细说明光阑孔径与FBG插入损耗和短波损耗之间的依赖关系，以0.5 mm为步长，将光阑孔径从10.0 mm逐步减小至0.5 mm，同样制备中心波长为1550 nm、反射率为90%的FBG，统计不同光阑孔径下FBG的插入损耗和1510 nm处的短波损耗，结果如图6所示。大体上以5.0 mm光阑孔径为转折点，两种损耗在光阑孔径大于5.0 mm时基本保持不变，在光阑孔径小于5.0 mm时开始逐步减小，在光阑孔径为1.0 mm时降低至最低，降至0.5 mm后又陡然增大。两种损耗的变化趋势与理论计算的光斑瑞利长度的变化趋势基本一致，由图2可以看出，当光阑孔径小于5.0 mm时，瑞利长度才开始逐步增大，表明此时光栅条纹也开始由圆形逐步向丝状过渡，损耗也开始逐步减小；直到光阑孔径减小至0.5 mm时，束腰半径的增大引起相邻光栅条纹出现了部分重叠，导致损耗再次增大。

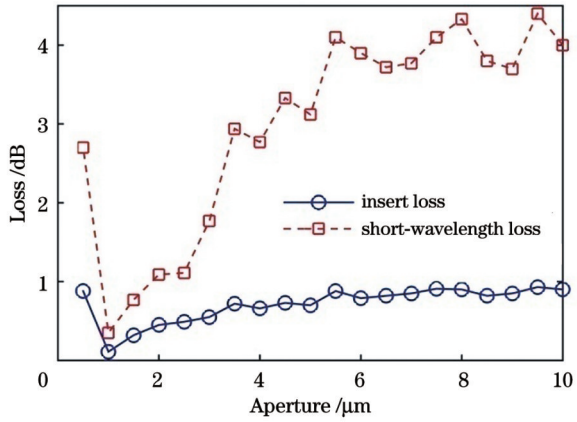

图6 不同光阑孔径下制备的FBG的插入损耗和短波损耗

Fig .6 Insertion loss and short-wavelength loss values of FBG fabricated with different apertures

FBG的短波损耗在较宽的光谱范围内以振荡的形式存在，这主要是由于光栅区域的折射率扰动激发了包层模，它们与光纤纤芯基模耦合[24]。包层模的有效折射率低于纤芯基模，因此耦合形成的干涉条纹集中在谐振谷值的短波侧；长波侧的光谱未受到影响，仍保持光源原有的平滑形态。振荡幅度主要取决于低方位角包层模的能量。当光阑孔径较大时，光栅条纹接近圆形，表面曲率高，激发出大量不同方位角的包层模，如图7(a)所示，其中高方位角包层模在传输过程中极易衰减，形成损耗，低方位角包层模与纤芯基模耦合，形成短波振荡。当光阑孔径降低至1.0 mm时，相比圆形条纹的高度局域化和高表面曲率，丝状条纹的折射率调制范围更大，表面曲率更低。这一方面降低了高方位角包层模的激发效率，使光能量的衰减减少，降低了FBG的损耗；另一方面，使某些特定低方位角包层模的激发获得加强，如图7(b)所示，包层模携带了更多的能量，从而与纤芯基模的耦合效率更高，因此此时短波损耗的振荡较大。

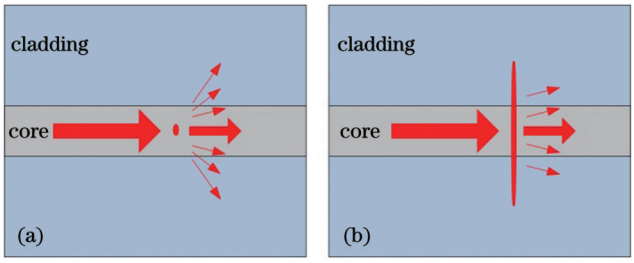

图7 包层模激发原理图。(a)圆形光栅条纹；(b)丝状光栅条纹

Fig. 7 Schematics of cladding mode coupling. (a) Circular grating fringe; (b) filamentous grating fringe

将FBG置于折射率匹配液中，包层模泄漏至匹配液中，不再与纤芯基模耦合，此时短波侧的光谱也变得平滑，如图8所示。由于匹配液折射率与光纤包层不能完美匹配，耦合未能完全消除，仍有局部小幅度的振荡现象。根据包层模的这一特点，可在保留涂覆层的光纤上制备FBG，以降低短波侧的振荡，如图9(a)所示。适当提高制备用的飞秒激光能量，以补偿其在涂覆层中的衰减[25]。也可采用较低的飞秒激光能量，制备低反射率(约40%)的FBG，降低包层模的激发效率，从而降低损耗和短波侧振荡，这同时也有助于压缩带宽，如图9(b)所示。

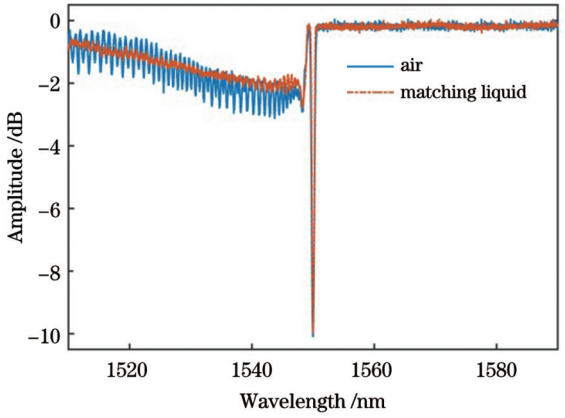

图8 空气中和匹配液中的FBG透射光谱

Fig. 8 FBG transmission spectra in air and matching liquid

4 结 论

提出了一种基于小孔径光阑整形的低损耗飞秒光纤光栅制备技术。对于光斑直径为10 mm的飞秒激光光束，在光阑孔径由10.0 mm降低至1.0 mm的过程中，光栅条纹形态由圆形逐步过渡至丝状，在垂直于飞秒激光入射方向上观察到的光栅条纹长度由1.74 μm提高至15.23 μm，小孔径光阑对光栅条纹起到丝状整

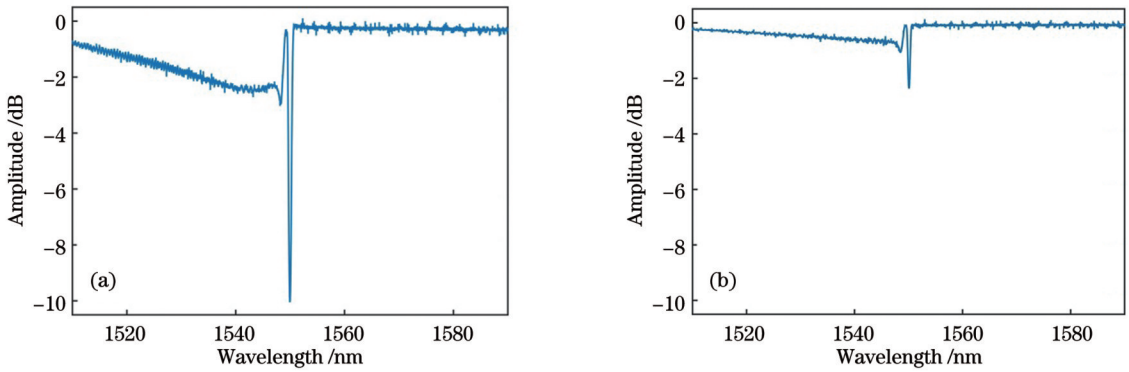

图 9 在短波侧振荡的FBG透射光谱。(a)在保留涂覆层的光纤上制备的FBG;(b)低反射率FBG

Fig. 9 FBG transmission spectra oscillating at short wavelength side. (a) FBG prepared on coated fiber; (b) low reflection

形效果。制备了中心波长为1550 nm、反射率为90%的FBG,插入损耗由0.90 dB降低至0.11 dB,1510 nm处的短波损耗由4.01 dB降低至0.35 dB,小孔径光阑整形对插入损耗和短波损耗产生显著的抑制效果。相比圆形光栅条纹,丝状光栅条纹的表面曲率更低,同时较低的折射率调制幅度可产生较高的耦合强度,降低了对入射激光的米氏散射,因此有效地降低了光栅的损耗。丝状条纹还加强了低方位角包层模的激发,使短波损耗的振荡更大,通过保留涂覆层或降低反射率能够降低振荡幅度。

参 考 文 献

[1] Zhao Y, He T Y, Chen M Q, et al. Ultra-short fiber Bragg grating composed of cascaded microchannels in a microprobe for refractive index measurement[J]. Journal of Lightwave Technology, 2023, 41(8): 2555-2561.

[2] Ji L T, Sun Q Q, Zhao S S, et al. High-resolution fiber grating pressure sensor with *in situ* calibration for deep sea exploration[J]. Optics Express, 2023, 31(6): 10358-10367.

[3] Zhang R L, Wu X, Hong L, et al. High-sensitivity fiber Bragg grating strain sensor of the substrate type[J]. Applied Optics, 2022, 61(35): 10567-10573.

[4] 廖常锐, 何俊, 王义平. 飞秒激光制备光纤布拉格光栅高温传感器研究[J]. 光学学报, 2018, 38(3): 0328009.
Liao C R, He J, Wang Y P. Study on high temperature sensors based on fiber Bragg gratings fabricated by femtosecond laser[J]. Acta Optica Sinica, 2018, 38(3): 0328009.

[5] Warren-Smith S C, Schartner E P, Nguyen L V, et al. Stability of grating-based optical fiber sensors at high temperature[J]. IEEE Sensors Journal, 2019, 19(8): 2978-2983.

[6] 董欣然, 王子安, 曾理, 等. 飞秒激光刻写布拉格光栅反射光谱特性研究[J]. 中国激光, 2023, 50(17): 1906001.
Dong X R, Wang Z A, Zeng L, et al. Study of the reflection spectral characteristics of FBGs fabricated by femtosecond laser phase mask technique[J]. Chinese Journal of Lasers, 2023, 50(17): 1906001.

[7] Ioannou A, Kalli K. Femtosecond laser inscribed fiber Bragg gratings based on precise spatial apodization[J]. Optics Letters, 2023, 48(7): 1826-1829.

[8] Guo Q, Zheng Z M, Wang B, et al. Femtosecond laser fabricated apodized fiber Bragg gratings based on energy regulation[J]. Photonics, 2021, 8(4): 110-118.

[9] Pan X P, Guo Q, Wu Y D, et al. Femtosecond laser inscribed chirped fiber Bragg gratings[J]. Optics Letters, 2021, 46(9): 2059-2062.

[10] 李昊, 王蒙, 武柏屹, 等. 基于飞秒激光制备的啁啾倾斜布拉格光纤光栅[J]. 光学学报, 2023, 43(5): 0536001.
Li H, Wang M, Wu B Y, et al. Fabrication of chirped and tilted fiber Bragg gratings with femtosecond laser[J]. Acta Optica Sinica, 2023, 43(5): 0536001.

[11] 熊贤伟, 陈胜平, 朱宏田, 等. 飞秒激光直写高反射率中红外光纤布拉格光栅[J]. 中国激光, 2022, 49(1): 0101014.
Xiong X W, Chen S P, Zhu H T, et al. High reflectivity mid-infrared fiber Bragg grating by femtosecond laser direct inscription method[J]. Chinese Journal of Lasers, 2022, 49(1): 0101014.

[12] Marshall G D, Williams R J, Jovanovic N, et al. Point-by-point written fiber-Bragg gratings and their application in complex grating designs[J]. Optics Express, 2010, 18(19): 19844-19859.

[13] Åslund M L, Nemanja N, Groothoff N, et al. Optical loss mechanisms in femtosecond laser-written point-by-point fibre Bragg gratings[J]. Optics Express, 2008, 16(18): 14248-13254.

[14] Zhou K M, Dubov M, Mou C B, et al. Line-by-line fiber Bragg grating made by femtosecond laser[J]. IEEE Photonics Technology Letters, 2010, 22(16): 1190-1192.

[15] Lu P, Mihailov S J, Ding H M, et al. Plane-by-plane inscription of grating structures in optical fibers[J]. Journal of Lightwave Technology, 2017, 36(4): 926-931.

[16] Theodosiou A, Lacraz A, Stassis A, et al. Plane-by-plane femtosecond laser inscription method for single-peak Bragg gratings in multimode CYTOP polymer optical fiber[J]. Journal of Lightwave Technology, 2017, 35(24): 5404-5410.

[17] Xu X Z, He J, He J, et al. Slit beam shaping for femtosecond laser point-by- point inscription of high-quality fiber Bragg gratings[J]. Journal of Lightwave Technology, 2021, 39(15): 5142-5148.

[18] Williams R J, Krämer R G, Nolte S, et al. Femtosecond direct-writing of low-loss fiber Bragg gratings using a continuous core-scanning technique[J]. Optics Letters, 2013, 38(11): 1918-1920.

[19] Liu X Y, Wang Y P, Li Z L, et al. Low short-wavelength loss fiber Bragg gratings inscribed in a small-core fiber by femtosecond laser point-by-point technology[J]. Optics Letters, 2019, 44(21): 5121-5124.

[20] 阿曼·亚里夫, 波奇·耶赫. 光子学: 现代通信光电子学[M]. 陈鹤鸣, 施伟华, 汪静丽, 等, 译. 6版. 北京: 电子工业出版社, 2014: 15-28.
Yariv A, Yeh P. Optical electronics in modern communications [M]. Chen H M, Shi W H, Wang J L, et al., Transl. 6th ed. Beijing: Electronic Industry Press, 2014: 15-28.

[21] Jovanovic N, Thomas J, Williams R J, et al. Polarization-dependent effects in point-by-point fiber Bragg gratings enable simple, linearly polarized fiber lasers[J]. Optics Express, 2009, 17(8): 6082-6095.

[22] Williams R J, Jovanovic N, Marshall G D, et al. Optimizing the net reflectivity of point-by-point fiber Bragg gratings: the role of scattering loss[J]. Optics Express, 2012, 20(12): 13451-13456.

[23] Erdogan T. Fiber grating spectra[J]. Journal of Lightwave Technology, 1997, 15(8): 1277-1294.

[24] Thomas J, Jovanovic N, Becker R G, et al. Cladding mode coupling in highly localized fiber Bragg gratings: modal properties and transmission spectra[J]. Optics Express, 2010, 19(1): 325-341.

[25] Martinez A, Khrushchev I Y, Bennion I. Direct inscription of Bragg gratings in coated fibers by an infrared femtosecond laser[J]. Optics Letters, 2006, 31(11): 1603-1605.

Fabrication of Low-Loss Femtosecond Fiber Bragg Gratings Based on Beam Shaping by Small Aperture

Zhang Penghao[1], Wu Hongbo[1], Chen Shuang[1], Jiang Wensong[2*], Zhang Li[1]

[1]*Changcheng Institute of Metrology & Measurement, Aviation Industry Corporation of China, LTD., Beijing* 100095, *China*;

[2]*Colloge of Metrology & Measurement Engineering , China Jiliang University, Hangzhou* 310018, *Zhejiang*, *China*

Abstract

Objective Fiber Bragg gratings (FBGs) fabricated by femtosecond laser have the advantages of light weight, high capacity wavelength division multiplexing, high mechanical strength, and excellent thermal stability. As a significant sensitive component of sensors, FBGs have been deployed widely in aerospace, nuclear power, metallurgy, bridges, and tunnels. One common method of their construction is directly writing FBGs point by point; however, this suffers from high loss. Various techniques have been proposed to reduce this loss, such as improving the writing path to line by line, shaping femtosecond laser beams, and selecting optical fibers with smaller core diameters. Despite reductions in loss, there remain deficiencies in their production, such as low fabrication efficiency and generality. In this study, an inscription method of FBG based on a small-aperture beam shaping technique has been proposed, which can be helpful for the efficient fabrication of low-loss FBGs.

Methods First, the energy distribution of a focused Gaussian beam limited by aperture is analyzed, and the aperture condition of the filamentary focal field is obtained. A femtosecond laser writing device based on small aperture shaping is then built. When the aperture is gradually reduced from 10.0 mm to 0.5 mm, a series of second-order FBGs are written on standard quartz single-mode fibers with the coating removed. The lengths of the FBGs are 3 mm, the reflectivities are approximately 90%, and the center wavelengths are near 1550 nm. The microscopic images of the FBG are obtained via a charge coupled device (CCD) camera along and perpendicular to the laser incidence direction. The corresponding transmission spectra are obtained by an FBG interrogator.

Results and Discussions As the aperture decreases, the length of the grating fringes perpendicular to the laser incidence direction increases significantly faster than along the incidence direction; the shapes of the grating fringes thus gradually change from elliptical to filamentous. When the aperture is 10.0 mm, the insertion loss and short-wavelength loss (at 1510 nm) are 0.9 dB and 4.01 dB, respectively; when the aperture is reduced to 1.0 mm, these two types of losses decrease to 0.11 dB and 0.35 dB, respectively (Fig. 5). This is because the filamentous grating fringe reduces the curvature of the typical circular fringe, leading to less Mie scattering of incident light. At the same time, because the area of the coupling between the filamentous grating fringes and the fundamental mode of the fiber is greater, the same coupling amplitude requires smaller refractive index modulation. Therefore, the small aperture has a significant suppression effect on losses. The short-wavelength loss of FBG manifests in the form of oscillation over a wide spectral range, mainly due to the excitation of cladding modes by refractive index perturbations in the grating region, which are coupled with the fundamental mode of the fiber core. The oscillation amplitude mainly depends on the energy of the low azimuth cladding mode. When the aperture is reduced to 1.0 mm, the filamentous fringes have a smooth refractive index modulation, resulting in the lower excitation of high-azimuth cladding modes but the higher excitation of some low-azimuth cladding modes (Fig. 7). The low-azimuth cladding modes carry more energy, resulting in higher coupling efficiency with the fundamental mode of the core. The oscillation is reduced by writing an FBG on a coated fiber or an FBG with a relatively low reflectivity (such as 40%; Fig. 9).

Conclusions In this study, a low-loss femtosecond fiber grating fabrication technology based on small aperture shaping is proposed. The filamentous shaping effect of the small aperture on the grating fringe is theoretically analyzed and experimentally demonstrated. A series of FBGs with a central wavelength of 1550 nm and a reflectivity of 90% are fabricated by using different apertures. As the aperture is reduced from 10.0 mm to 1.0 mm, the grating fringe shape gradually transitions from circular to filamentous, while the insertion loss is reduced from 0.90 dB to 0.11 dB and the short-wavelength loss is reduced from 4.01 dB to 0.35 dB. Compared to circular grating fringes, the filamentous grating fringes reduce the Mie scattering of incident light and enhance the coupling of fundamental modes of the core, effectively reducing loss. The filamentous fringes also enhance the excitation of low-azimuth cladding modes, leading to greater oscillations at the short-wavelength side. These oscillations can be effectively suppressed by writing an FBG on a coated fiber or an FBG with a relatively low reflection.

Key words gratings; fiber Bragg gratings; femtosecond laser; small aperture; insertion loss; short-wavelength loss